

Low-Energy Effective Hamiltonian for Giant-Gap Quantum Spin Hall Insulators in Honeycomb X-Hydride/Halide (X=N-Bi) Monolayers

Cheng-Cheng Liu,¹ Shan Guan,¹ Zhigang Song,² Shengyuan A. Yang,³ Jinbo Yang,^{2,4} and Yugui Yao¹

¹*School of Physics, Beijing Institute of Technology, Beijing 100081, China*

²*State Key Laboratory for Mesoscopic Physics, and School of Physics, Peking University, Beijing 100871, China*

³*Engineering Product Development, Singapore University of Technology and Design, Singapore 138682, Singapore*

⁴*Collaborative Innovation Center of Quantum Matter, Beijing, China*

From the tight-binding method in combination with first-principles calculation, we systematically derived the low-energy effective Hilbert subspace and Hamiltonian involving spin-orbit coupling for two-dimensional honeycomb hydrogenated and halogenated group V systems. These materials are proposed as giant-gap quantum spin Hall insulators, for example with record huge bulk band gaps opened by spin-orbit coupling at the Dirac points from 0.74 eV to 1.08 eV in BiX (X=H, F, Cl, and Br) monolayer. We found that the low-energy Hilbert subspace mainly consists of p_x and p_y orbitals from the group V elements, and the giant first order effective intrinsic spin-orbit coupling is from on site spin-orbit interaction. These features are quite distinct from the typical Kane-Mele model describing group IV monolayers such as graphene and silicene. There the relevant orbital is p_z and the effective intrinsic spin-orbit coupling is from next-nearest-neighbor spin-orbit interaction processes. These systems represent the first real 2D honeycomb lattice materials in which the low-energy physics is associated with p_x and p_y orbitals. A spinful lattice Hamiltonian with the on site SOC term for these systems is derived, which could facilitate further investigations of these intriguing materials.

PACS numbers: 73.43.-f, 73.22.-f, 71.70.Ej, 85.75.-d

I. INTRODUCTION

Recent years have witnessed great interest in the two-dimensional (2D) layered materials with honeycomb structures. Especially, the 2D group IV honeycomb lattice materials, such as successively fabricated graphene^{1,2}, and silicene^{3,4}, have attracted considerable attention both theoretically and experimentally due to their low-energy Dirac electronic behaviors and promising applications in electronics. Currently, we have found stable 2D hydrogenated and halogenated group V honeycomb lattices via first-principles (FP) calculations of structure optimization, finite temperature molecular dynamics, and phonon modes⁵. The structures are similar to that of a hydrogenated silicene (silicane), as shown in Fig. 1(a). In the absence of spin-orbit coupling (SOC), the band structures show linear energy spectrum crossing at the Fermi level around K and K' points of the hexagonal Brillouin zone. The honeycomb optical lattice in cold atoms system involving p_x and p_y orbitals are also very interesting, where various charge, bond, and orbital ordered states as well as quantum anomalous Hall effects were proposed⁶⁻⁸. These 2D hydrogenated and halogenated group V honeycomb materials represent the first true 2D honeycomb lattice condensed matters in which the low-energy physics is associated with p_x and p_y orbitals.

When taking into account the SOC, a mass term can be introduced, which results in the nontrivial band topology, and the system turns into a quantum spin Hall insulator. Quantum spin Hall (QSH) effect, a novel quantum state of matter with nontrivial topological property, has garnered great interest in the fields of con-

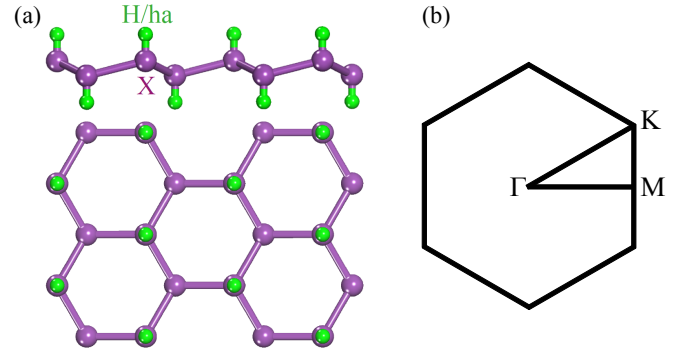


FIG. 1. (color online). (a) The lattice geometry for 2D X-hydride/halide (X=N-Bi) monolayer from the side view (upper) and top view (lower). Note that two sets of sublattice in the honeycomb group V element X are not coplanar and buckled, which are hydrogenated or halogenated from both sides. (b) The first Brillouin zone of 2D X-hydride/halide (X=N-Bi) monolayer and the points of high symmetry.

densed matter physics and materials science due to its scientific importance as a novel quantum state and potential technological applications ranging from spintronics to topological quantum computation⁹⁻¹¹. This novel electronic state with time reversal invariance is gaped in the bulk and conducts charge and spin in gapless edge states without dissipation at the sample boundaries. The concept of QSH effect was first proposed by Kane and Mele in graphene in which SOC opens a nontrivial band gap at the Dirac points^{12,13}. Subsequent works, however, showed that the SOC is rather weak, which is in fact a second order process of the atomic spin

orbit interaction for graphene, hence the effect is difficult to be detected in graphene experimentally^{14,15}. So far, QSH effect has only been successfully demonstrated in HgTe/CdTe quantum wells^{16,17}, and experimental evidence for helical edge modes has been presented for inverted InAs-GaSb quantum wells^{18–20}. Nevertheless, HgTe quantum wells and other systems more or less have serious limitations like toxicity, difficulty in processing, and small bulk gap opened by SOC. Therefore, an easy and environmentally friendly realization of QSH effect is much desired. Extensive effort has been devoted to search for new QSH insulators with large SOC gap^{21–28}. For instance, new layered honeycomb lattice type materials such as silicene, germanene²⁴ or stanene²⁵, and chemically modified stanene²⁷ have been proposed. Ultrathin Bi(111) films have drawn attention as a candidate QSH insulator, whose 2D topological properties have been reported²⁹. Recently, an approach is proposed to design large-gap quantum spin Hall state on a semiconductor surface by substrate orbital filtering process³⁰. However, the desirable QSH insulators preferably with huge bulk gaps are still rare. A sizable bulk band gap in QSH insulators is essential for realizing many exotic phenomena and fabricating new quantum devices that can operate at room temperature.

Using the FP method, we have recently demonstrated that the QSH effect can be realized in the 2D hydrogenated and halogenated group V honeycomb monolayers, with a huge gap opened at the Dirac points due to the SOC⁵, which are promising candidates for constructing novel spintronic devices. Although the low energy spectrum of these materials are similar to those of the 2D group IV honeycomb monolayers such as graphene and silicene, the low-energy Hilbert space changes from the p_z orbital to the orbitals mainly consisted of p_x and p_y . Moreover, the nature of the effective SOC differs between the two systems. Motivated by the fundamental interest associated with QSH effect and huge effective SOC gap in the 2D group V honeycomb monolayers, we attempt to derive a low-energy effective model Hamiltonian for these materials which captures the essential physics. Such a model will be useful for further studies of their interesting properties.

Based on the symmetry arguments, the next-nearest-neighbor (NNN) intrinsic Rashba SOC should exist in these systems due to the low-buckled structure, similar to the case of silicene²⁵. However, as we shall see, the dominant effect is from the much larger first order SOC of on site origin. Therefore, in the following discussion, we shall focus on the first order on site SOC and neglect the higher order effects. This point will be further discussed later in this paper.

The paper is organized as follows. In Sec. II, we derive the low-energy effective Hilbert subspace and Hamiltonian for honeycomb X-hydride (X=N-Bi) monolayers step-by-step, and also investigate in detail the effective SOC. Section III presents the derivation of the low-energy effective model involving SOC for X-halide (X=N-Bi,

halide=F-I) honeycomb monolayers. In Sec. IV, a simple spinful lattice Hamiltonian for the honeycomb X-hydride/halide (X=N-Bi) monolayers is derived. We conclude in Sec. V with a brief discussion and summary.

II. LOW-ENERGY EFFECTIVE HAMILTONIAN FOR HONEYCOMB XH(X=N-BI) MONOLAYERS

A. Low-energy Hilbert subspace and effective Hamiltonian without SOC

In the following analytic study, the outer shell orbitals of X (X=N-Bi), namely s , p_x , p_y , p_z , and s orbital of H are taken into consideration. As is shown in Fig. 1(a), there are two distinct sites A and B in the unit cell of X-hydride (X=N-Bi) honeycomb lattice with full hydrogenation from both sides of the 2D X honeycomb sheet. Therefore, in the representation $\{|p_y^A\rangle, |p_x^A\rangle, |p_z^A\rangle, |s_H^A\rangle, |s^A\rangle, |p_y^B\rangle, |p_x^B\rangle, |p_z^B\rangle, |s_H^B\rangle, |s^B\rangle\}$ (For simplicity, the Dirac ket is then omitted in the following) and at the K point, the total Hamiltonian with the nearest neighbor hopping considered in the Slater-Koster formalism (Appendix A) reads

$$H_0 = \begin{pmatrix} H_0^{11} & H_0^{12} \\ H_0^{12\dagger} & H_0^{22} \end{pmatrix}, \quad (1)$$

$$H_0^{11} = \begin{pmatrix} 0 & 0 & 0 & 0 & 0 \\ 0 & 0 & 0 & 0 & 0 \\ 0 & 0 & 0 & -V_{sp\sigma}^H & 0 \\ 0 & 0 & -V_{sp\sigma}^H & \Delta_H & V_{ss\sigma}^H \\ 0 & 0 & 0 & V_{ss\sigma}^H & \Delta \end{pmatrix}, \quad (2)$$

$$H_0^{12} = \begin{pmatrix} -V_1' & -iV_1' & 0 & 0 & V_2' \\ -iV_1' & V_1' & 0 & 0 & -iV_2' \\ 0 & 0 & 0 & 0 & 0 \\ 0 & 0 & 0 & 0 & 0 \\ -V_2' & iV_2' & 0 & 0 & 0 \end{pmatrix}, \quad (3)$$

$$H_0^{22} = \begin{pmatrix} 0 & 0 & 0 & 0 & 0 \\ 0 & 0 & 0 & 0 & 0 \\ 0 & 0 & 0 & V_{sp\sigma}^H & 0 \\ 0 & 0 & V_{sp\sigma}^H & \Delta_H & V_{ss\sigma}^H \\ 0 & 0 & 0 & V_{ss\sigma}^H & \Delta \end{pmatrix}, \quad (4)$$

where $V_{sp\sigma}^H$ ($V_{ss\sigma}^H$) is the hopping between the p_z (s) orbital from X and the s orbital from H. V_1' and V_2' can be expressed by the Slater-Koster parameters (Eq. (A5)). Δ and Δ_H are on site energies for s orbitals of X and H, respectively. The on site energies for p_x , p_y , and p_z orbitals are taken to be zero.

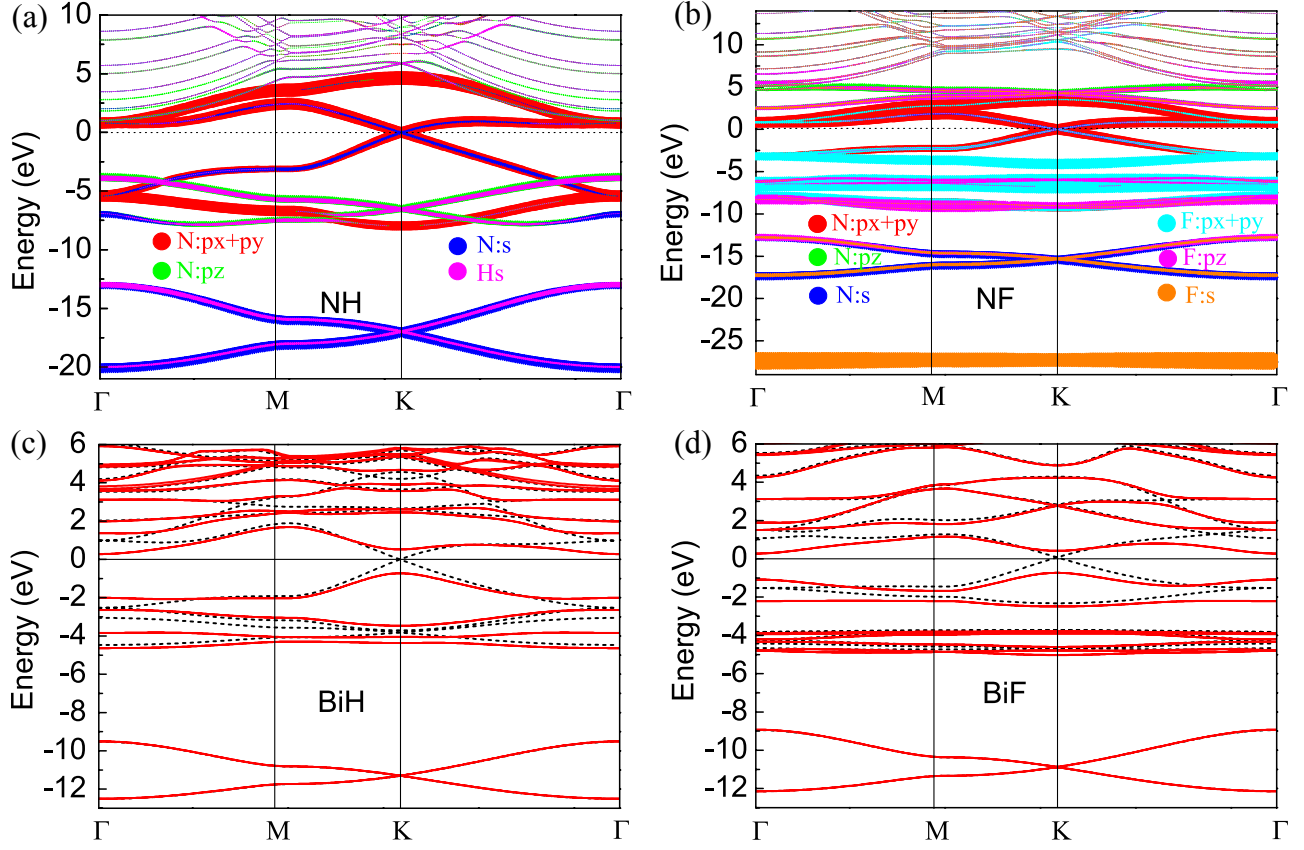


FIG. 2. (color online). (a)(b) The partial band structure projection for NH and NF without SOC, respectively. Symbol size is proportional to the population in the corresponding states. The Fermi level is indicated by the dotted line. (c)(d) Band structures for BiH and BiF without (black dash lines) and with (red solid lines) SOC. The Fermi level is indicated by the solid line.

To diagonalize the total Hamiltonian, we firstly perform the following unitary transformation,

$$\begin{aligned}
 \varphi_1^A &= -\frac{1}{\sqrt{2}} (p_x^A + ip_y^A) = |p_+^A\rangle, \\
 \varphi_2^B &= \frac{1}{\sqrt{2}} (p_x^B - ip_y^B) = |p_-^B\rangle, \\
 \varphi_3 &= \frac{1}{\sqrt{2}} \left[-\frac{1}{\sqrt{2}} (p_x^A - ip_y^A) - \frac{1}{\sqrt{2}} (p_x^B + ip_y^B) \right], \\
 \varphi_4 &= \frac{1}{\sqrt{2}} \left[\frac{1}{\sqrt{2}} (p_x^A - ip_y^A) - \frac{1}{\sqrt{2}} (p_x^B + ip_y^B) \right].
 \end{aligned} \tag{5}$$

We rewrite the total Hamiltonian in the new basis $\{\varphi_1^A, \varphi_2^B, \varphi_3, \varphi_4, p_z^A, s_H^A, s^A, p_z^B, s_H^B, s^B\}$

$$H_0 \longrightarrow H_1 = U_1^\dagger H_0 U_1, \tag{6}$$

$$H_1 = \begin{pmatrix} H_1^{11} & H_1^{12} \\ H_1^{12\dagger} & H_1^{22} \end{pmatrix}, \tag{7}$$

$$H_1^{11} = \begin{pmatrix} 0 & 0 & 0 & 0 & 0 \\ 0 & 0 & 0 & 0 & 0 \\ 0 & 0 & V_1 & 0 & 0 \\ 0 & 0 & 0 & -V_1 & 0 \\ 0 & 0 & 0 & 0 & 0 \end{pmatrix}, \tag{8}$$

$$H_1^{12} = \begin{pmatrix} 0 & 0 & 0 & 0 & iV_2 \\ 0 & -iV_2 & 0 & 0 & 0 \\ 0 & 0 & 0 & 0 & 0 \\ 0 & 0 & 0 & 0 & 0 \\ -V_{sp\sigma}^H & 0 & 0 & 0 & 0 \end{pmatrix}, \tag{9}$$

$$H_1^{22} = \begin{pmatrix} \Delta_H & V_{ss\sigma}^H & 0 & 0 & 0 \\ V_{ss\sigma}^H & \Delta & 0 & 0 & 0 \\ 0 & 0 & 0 & V_{sp\sigma}^H & 0 \\ 0 & 0 & V_{sp\sigma}^H & \Delta_H & V_{ss\sigma}^H \\ 0 & 0 & 0 & V_{ss\sigma}^H & \Delta \end{pmatrix}, \tag{10}$$

$$U_1 = \begin{pmatrix} \frac{-i}{\sqrt{2}} & 0 & \frac{i}{2} & \frac{-i}{2} & 0 & 0 & 0 & 0 & 0 & 0 \\ \frac{-1}{\sqrt{2}} & 0 & \frac{-1}{2} & \frac{1}{2} & 0 & 0 & 0 & 0 & 0 & 0 \\ 0 & 0 & 0 & 0 & 1 & 0 & 0 & 0 & 0 & 0 \\ 0 & 0 & 0 & 0 & 0 & 1 & 0 & 0 & 0 & 0 \\ 0 & 0 & 0 & 0 & 0 & 0 & 1 & 0 & 0 & 0 \\ 0 & \frac{-i}{\sqrt{2}} & \frac{-i}{2} & \frac{-i}{2} & 0 & 0 & 0 & 0 & 0 & 0 \\ 0 & \frac{1}{\sqrt{2}} & \frac{-1}{2} & \frac{-1}{2} & 0 & 0 & 0 & 0 & 0 & 0 \\ 0 & 0 & 0 & 0 & 0 & 0 & 0 & 1 & 0 & 0 \\ 0 & 0 & 0 & 0 & 0 & 0 & 0 & 0 & 1 & 0 \\ 0 & 0 & 0 & 0 & 0 & 0 & 0 & 0 & 0 & 1 \end{pmatrix}, \quad (11)$$

where $V_1 = 2V_1'$ and $V_2 = \sqrt{2}V_2'$.

The new basis can be rearranged in the order as $\{\varphi_1^A, s^B, s_H^B, p_z^B, \varphi_2^B, s^A, s_H^A, p_z^A, \varphi_3, \varphi_4\}$. After that, the total Hamiltonian can be written as a block diagonal form with three decoupled blocks H_α , H_β , and H_γ :

$$H_1 \longrightarrow H_2 = U_2^\dagger H_1 U_2, \quad (12)$$

$$U_2 = \begin{pmatrix} 1 & 0 & 0 & 0 & 0 & 0 & 0 & 0 & 0 & 0 \\ 0 & 0 & 0 & 0 & 1 & 0 & 0 & 0 & 0 & 0 \\ 0 & 0 & 0 & 0 & 0 & 0 & 0 & 0 & 1 & 0 \\ 0 & 0 & 0 & 0 & 0 & 0 & 0 & 0 & 0 & 1 \\ 0 & 0 & 0 & 0 & 0 & 0 & 0 & 1 & 0 & 0 \\ 0 & 0 & 0 & 0 & 0 & 0 & 1 & 0 & 0 & 0 \\ 0 & 0 & 0 & 0 & 0 & 1 & 0 & 0 & 0 & 0 \\ 0 & 0 & 0 & 1 & 0 & 0 & 0 & 0 & 0 & 0 \\ 0 & 0 & 1 & 0 & 0 & 0 & 0 & 0 & 0 & 0 \\ 0 & 1 & 0 & 0 & 0 & 0 & 0 & 0 & 0 & 0 \end{pmatrix}, \quad (13)$$

$$H_2 = H_\alpha \oplus H_\beta \oplus H_\gamma, \quad (14)$$

with

$$H_\alpha = \begin{pmatrix} 0 & iV_2 & 0 & 0 \\ -iV_2 & \Delta & V_{ss\sigma}^H & 0 \\ 0 & V_{ss\sigma}^H & \Delta_H & V_{sp\sigma}^H \\ 0 & 0 & V_{sp\sigma}^H & 0 \end{pmatrix}, \quad (15)$$

$$H_\beta = \begin{pmatrix} 0 & -iV_2 & 0 & 0 \\ iV_2 & \Delta & V_{ss\sigma}^H & 0 \\ 0 & V_{ss\sigma}^H & \Delta_H & -V_{sp\sigma}^H \\ 0 & 0 & -V_{sp\sigma}^H & 0 \end{pmatrix}, \quad (16)$$

$$H_\gamma = \text{diag}\{V_1, -V_1\}. \quad (17)$$

The eigenvectors for the first diagonal block H_α can be written as

$$|\varepsilon_i\rangle = \frac{1}{N_i} \begin{pmatrix} 1 \\ -i\frac{\varepsilon_i}{V_2} \\ -i\frac{\varepsilon_i^2 - \Delta\varepsilon_i - V_2^2}{V_2 V_{ss\sigma}^H} \\ -i\frac{V_{sp\sigma}^H}{\varepsilon_i} \frac{\varepsilon_i^2 - \Delta\varepsilon_i - V_2^2}{V_2 V_{ss\sigma}^H} \end{pmatrix}, \quad (18)$$

where ε_i and N_i ($i = 1 - 4$) are the corresponding eigenvalues and normalization factors, respectively.

Therefore, upon performing the unitary transformation $\{\phi_1, \phi_2, \phi_3, \phi_4\} = \{\varphi_1^A, s^B, s_H^B, p_z^B\} U_\alpha$ with $U_\alpha = \{|\varepsilon_i\rangle\}_{i=1-4} \equiv \{u_{ji}^\alpha\}$, the above upper-left 4×4 diagonal block has been diagonalized.

For the second diagonal block H_β , its eigenvalues are denoted as ε_{4+i} ($i = 1 - 4$), and satisfy $\varepsilon_{4+i} = \varepsilon_i$ ($i = 1 - 4$), where ε_i ($i = 1 - 4$) are eigenvalues of H_α , since the diagonal blocks H_α and H_β have the same eigenequations. This is consistent with the FP calculations, i.e. there are four two-fold degeneracy points at K point as shown in Fig. 2(a). The eigenvectors of H_β are

$$|\varepsilon_i\rangle = \frac{1}{N_i} \begin{pmatrix} 1 \\ i\frac{\varepsilon_i}{V_2} \\ i\frac{\varepsilon_i^2 - \Delta\varepsilon_i - V_2^2}{V_2 V_{ss\sigma}^H} \\ -i\frac{V_{sp\sigma}^H}{\varepsilon_i} \frac{\varepsilon_i^2 - \Delta\varepsilon_i - V_2^2}{V_2 V_{ss\sigma}^H} \end{pmatrix}, \quad (19)$$

with ε_i and N_i ($i = 5 - 8$) the corresponding eigenvalues and the normalization factors. Similar to the case of H_α , upon performing the unitary transformation $\{\phi_5, \phi_6, \phi_7, \phi_8\} = \{\varphi_2^B, s^A, s_H^A, p_z^A\} U_\beta$ with $U_\beta = \{|\varepsilon_{i+4}\rangle\}_{i=1-4} \equiv \{u_{ji}^\beta\}$, the above diagonal block H_β has been diagonalized.

For the third diagonal block H_γ with eigenvalues $\{V_1, -V_1\}$ and eigenvectors $\{\varphi_3, \varphi_4\} \equiv \{\phi_9, \phi_{10}\}$, it is a diagonal matrix. Therefore, in the new basis $\{\phi_1, \phi_2, \phi_3, \phi_4, \phi_5, \phi_6, \phi_7, \phi_8, \phi_9, \phi_{10}\} = \{\varphi_1^A, s^B, s_H^B, p_z^B, \varphi_2^B, s^A, s_H^A, p_z^A, \varphi_3, \varphi_4\} U_3$, where $U_3 \equiv u^\alpha \oplus u^\beta \oplus I_{2 \times 2}$, the total Hamiltonian Eq. (1) takes a fully diagonalized form. The whole diagonalization process can be summarized as follow

$$\begin{aligned} & \{\phi_1, \phi_2, \phi_3, \phi_4, \phi_5, \phi_6, \phi_7, \phi_8, \phi_9, \phi_{10}\} \\ & = \{p_y^A, p_x^A, p_z^A, s_H^A, s^A, p_y^B, p_x^B, p_z^B, s_H^B, s^B\} U, \end{aligned} \quad (20)$$

$$U = U_1 U_2 U_3, \quad (21)$$

$$H_0 \longrightarrow H'_0 = U^\dagger H_0 U, \quad (22)$$

$$H'_0 = \text{diag}\{\varepsilon_1, \varepsilon_2, \varepsilon_3, \varepsilon_4, \varepsilon_5, \varepsilon_6, \varepsilon_7, \varepsilon_8, V_1, -V_1\}. \quad (23)$$

From the band components projection as shown in Fig. 2(a), in the vicinity of the Dirac points and the Fermi level, the main components of the band come from the p_x and p_y orbitals of group V element X, mixed with a small amount of s orbital of X as well as other orbitals. Compared with the expressions of the eigenstates obtained above, we find that the orbital features agree with that of $|\varepsilon_1\rangle$ and $|\varepsilon_1\rangle$ if we take their eigenenergies as the Fermi energy. Therefore states ϕ_1 and ϕ_5 constitute the low-energy Hilbert subspace. In the following, we will give explicit forms of the low-energy states ϕ_1 and ϕ_5 as well as their eigenvalues ε_1 .

Notice that, in the above 4×4 H_α , the scale of the 2×2 non-diagonal block $H_{\alpha 12}$ is smaller than the difference of the typical eigenvalues between the upper-left 2×2 diagonal block $H_{\alpha 11}$ and the lower-right 2×2 diagonal block $H_{\alpha 22}$ for the XH (X=N-Bi) systems. Using the definition of the Green function $(\varepsilon - H_\alpha)G = I$, with the matrix form

$$\begin{pmatrix} \varepsilon - H_{\alpha 11} & -H_{\alpha 12} \\ -H_{\alpha 21} & \varepsilon - H_{\alpha 22} \end{pmatrix} \begin{pmatrix} G_{11} & G_{12} \\ G_{21} & G_{22} \end{pmatrix} = I, \quad (24)$$

we obtain $[\varepsilon - H_{\alpha 11} - H_{\alpha 12}(\varepsilon - H_{\alpha 22})^{-1}H_{\alpha 21}]G_{11} = I$. Therefore the low energy effective Hamiltonian reads

$$H_{\alpha 11}^{eff} = H_{\alpha 11} + H_{\alpha 12}(\varepsilon - H_{\alpha 22})^{-1}H_{\alpha 21}. \quad (25)$$

up to the second order, one obtain

$$\varepsilon_1 = \frac{1}{2} \left(\Delta' + \sqrt{\Delta'^2 + 4V_2^2} \right), \quad (26)$$

with

$$\Delta' = \Delta + \frac{\varepsilon V_{ss\sigma}^H}{\varepsilon^2 - \Delta_H \varepsilon - V_{sp\sigma}^H}, \quad \varepsilon = \frac{1}{2} \left(\Delta + \sqrt{\Delta^2 + 4V_2^2} \right). \quad (27)$$

Consequently, we can obtain the explicit expressions of $|\varepsilon_1\rangle \equiv \{u_{j1}^\alpha\}_{j=1,4}$ and ϕ_1 . In the similar way, the explicit expressions of $|\varepsilon_5\rangle \equiv \{u_{j1}^\beta\}_{j=1,4}$ and ϕ_5 can also be obtained. So far, we have obtained the eigenvalues $\varepsilon_1 = \varepsilon_5$ (Eqs. (26) (27)) and the corresponding low energy Hilbert subspace consisted of ϕ_1 and ϕ_5 ,

$$\begin{aligned} \phi_1 &= u_{11}^\alpha \varphi_1^A + u_{21}^\alpha s^B + u_{31}^\alpha s_H^B + u_{41}^\alpha p_z^B, \\ \phi_5 &= u_{11}^\alpha \varphi_2^B - u_{21}^\alpha s^A - u_{31}^\alpha s_H^A + u_{41}^\alpha p_z^A. \end{aligned} \quad (28)$$

The above coefficients $\{u_{j1}^\alpha\}_{j=1,4}$ are given in Eq. (18) with ε_1 known.

Further simplification could be made in order to capture the main physics. We can omit the second order correction for the eigenvalues and the first order correction for the eigenvectors, i.e. the parts $u_{31}^\alpha s_H^B + u_{41}^\alpha p_z^B$ for ϕ_1 and $-u_{31}^\alpha s_H^A + u_{41}^\alpha p_z^A$ for ϕ_5 , and only keep the zero order eigenvectors and eigenvalues,

$$\begin{aligned} \phi_1 &= u_{11}^\alpha \varphi_1^A + u_{21}^\alpha s^B, \\ \phi_5 &= u_{11}^\alpha \varphi_2^B - u_{21}^\alpha s^A, \\ \varepsilon_1 = \varepsilon &= \frac{1}{2} \left(\Delta + \sqrt{\Delta^2 + 4V_2^2} \right). \end{aligned} \quad (29)$$

This is consistent with our FP calculations, namely in the vicinity of the Fermi level, p_x , p_y and s orbitals overwhelmingly dominate over the s_H and p_z orbital in the band components.

Meanwhile, the above Hamiltonian (Eq. (23)) can be rewritten as $H'_0 = E_F \cdot I_{10 \times 10} + H''_0$. When the Fermi energy $E_F = \varepsilon_1$ is taken as energy zero

point, we obtain the final form of the Hamiltonian (Eq. (1)) at the Dirac K point in the representation $\{\phi_1, \phi_2, \phi_3, \phi_4, \phi_5, \phi_6, \phi_7, \phi_8, \phi_9, \phi_{10}\}$

$$H''_0 = \text{diag}[0, \varepsilon_2 - \varepsilon_1, \varepsilon_3 - \varepsilon_1, \varepsilon_4 - \varepsilon_1, 0, \varepsilon_6 - \varepsilon_1, \varepsilon_7 - \varepsilon_1, \varepsilon_8 - \varepsilon_1, V_1 - \varepsilon_1, -V_1 - \varepsilon_1]. \quad (30)$$

The low-energy states ϕ_1 and ϕ_5 , which constitute the low-energy Hilbert subspace, have explicit forms after the above procedures of simplification

$$\begin{aligned} \phi_1 &= u_{11}^\alpha \left[-\frac{1}{\sqrt{2}} (p_x^A + ip_y^A) \right] + u_{21}^\alpha s^B, \\ \phi_5 &= u_{11}^\alpha \left[\frac{1}{\sqrt{2}} (p_x^B - ip_y^B) \right] - u_{21}^\alpha s^A, \end{aligned} \quad (31)$$

with

$$\begin{aligned} u_{11}^\alpha &= \frac{i \left(-\Delta + \sqrt{\Delta^2 + 18V_{sp\sigma}^2} \right)}{\sqrt{2\Delta^2 + 36V_{sp\sigma}^2 - 2\Delta\sqrt{\Delta^2 + 18V_{sp\sigma}^2}}}, \\ u_{21}^\alpha &= \frac{2V_2}{\sqrt{2\Delta^2 + 36V_{sp\sigma}^2 - 2\Delta\sqrt{\Delta^2 + 18V_{sp\sigma}^2}}}. \end{aligned}$$

We are interested in the low-energy physics near the Dirac point K , hence we perform the small \vec{k} expansion in the above low-energy Hilbert subspace around K by $\vec{k} \rightarrow \vec{k} + K$ and keep the first order term of \vec{k} ,

$$H_K = \begin{pmatrix} 0 & v_F k_- \\ v_F k_+ & 0 \end{pmatrix}, \quad (32)$$

with v_F being the Fermi velocity

$$v_F = \frac{\sqrt{3}a}{2} \left[\frac{1}{2} |u_{11}^\alpha|^2 (V_{pp\sigma} - V_{pp\pi}) + u_{21}^{\alpha 2} V_{ss\sigma} \right], \quad (33)$$

$$k_+ = k_x + ik_y, k_- = k_x - ik_y.$$

Through the analogical operations, we can also obtain the low-energy Hilbert subspace around the K'

$$\begin{aligned} \phi_1 &= u_{11}^\alpha \left[-\frac{1}{\sqrt{2}} (p_x^A - ip_y^A) \right] - u_{21}^\alpha s^B, \\ \phi_5 &= u_{11}^\alpha \left[\frac{1}{\sqrt{2}} (p_x^B + ip_y^B) \right] + u_{21}^\alpha s^A, \end{aligned} \quad (34)$$

and the low-energy effective Hamiltonian

$$H_{K'} = \begin{pmatrix} 0 & v_F k_+ \\ v_F k_- & 0 \end{pmatrix}. \quad (35)$$

The low-energy effective Hamiltonian around the Dirac points K and K' are related by time reversal and space

inversion symmetries. Finally, the low-energy Hilbert subspace can be chosen as

$$\begin{aligned}\phi_1 &= u_{11}^\alpha \left[-\frac{1}{\sqrt{2}} (p_x^A + i\tau_z p_y^A) \right] + u_{21}^\alpha \tau_z s^B, \\ \phi_5 &= u_{11}^\alpha \left[\frac{1}{\sqrt{2}} (p_x^B - i\tau_z p_y^B) \right] - u_{21}^\alpha \tau_z s^A,\end{aligned}\quad (36)$$

and the low-energy effective Hamiltonian without SOC reads

$$H_\tau = v_F (k_x \sigma_x + \tau_z k_y \sigma_y), \quad (37)$$

where Pauli matrix σ denotes orbital basis degrees of freedom ϕ_1 and ϕ_5 , and $\tau_z = \pm 1$ labels valley index K and K' . Note that under the space inversion operation $P = \sigma_x \tau_x$ and the time reversal operation $T = \tau_x \hat{K}$ with complex conjugation operator \hat{K} , the above low-energy effective Hamiltonian (Eq. (37)) is invariant.

B. Low-energy effective Hamiltonian involving SOC

From the Dirac equation, the following SOC term³¹ can be obtained

$$H_{so} = \frac{\hbar}{4m_0^2 c^2} (\nabla V \times \vec{p}) \cdot \vec{s} \quad (38)$$

where V is potential energy, \vec{p} is momentum, \hbar is Plank's constant, m_0 is the mass of a free electron, c is speed of light, \vec{s} is the vector of Pauli matrices. In a central potential, the SOC term could be written as

$$H_{so} = \xi_0 \hat{L} \cdot \hat{s} = \frac{\xi_0}{2} \left(\frac{L_+ s_- + L_- s_+}{2} + L_z s_z \right), \quad (39)$$

where $s_\pm = s_x \pm i s_y$ and $L_\pm = L_x \pm i L_y$ denote the ladder operators for the spin and orbital angular momenta, respectively. Here $\hat{s} = \frac{\hbar}{2} \vec{s}$, and in the following we take $\hbar = 1$. ξ_0 is the magnitude of atomic SOC. During the derivation we may take advantage of the following expressions

$$\begin{aligned}L_+ |l, m\rangle &= [l(l+1) - m(m+1)]^{1/2} |l, m+1\rangle, \\ L_- |l, m\rangle &= [l(l+1) - m(m-1)]^{1/2} |l, m-1\rangle, \\ L_z |l, m\rangle &= m |l, m\rangle,\end{aligned}\quad (40)$$

where l, m represent the azimuthal quantum number and magnetic quantum number, respectively. A straightforward calculation leads to the on site SOC in the spinfull low-energy Hilbert subspace (Eq. (36)) $\{\phi_1, \phi_5\} \otimes \{\uparrow, \downarrow\}$,

$$H_{so} = \lambda_{so} \tau_z \sigma_z s_z, \quad (41)$$

$$\begin{aligned}\lambda_{so} &= \frac{1}{2} |u_{11}^\alpha|^2 \xi_0 \\ &= \frac{1}{2} \left[1 - \frac{9V_{sp\sigma}^2}{\Delta^2 - \Delta \sqrt{\Delta^2 + 18V_{sp\sigma}^2 + 18V_{sp\sigma}^2}} \right] \xi_0.\end{aligned}\quad (42)$$

TABLE I. The parameters Fermi velocity v_F and magnitude of intrinsic effective SOC λ_{so} for honeycomb X-hydride (X=N-Bi) monolayers, which are obtained from FP calculations. Note that $\lambda_{so} = E_g/2$, with E_g gap opened by SOC at the Dirac point.

system	v_F ($10^5 m/s$)	λ_{so} (eV)
NH	6.8	6.7×10^{-3}
PH	8.3	18×10^{-3}
AsH	8.7	97×10^{-3}
SbH	8.6	0.21
BiH	8.9	0.62

It should be noted that in the honeycomb X-hydride (X=N-Bi) monolayers the dominant first order intrinsic effective SOC is on site rather than the NNN SOC term in the Kane-Mele model.

Consequently, from the above Hamiltonian Eqs. (37) and (41), we obtain the generic low-energy effective Hamiltonian around the Dirac points acting on the low-energy Hilbert subspace (Eq. (36)) $\{\phi_1, \phi_5\} \otimes \{\uparrow, \downarrow\}$

$$H_{eff} = H_\tau + H_{so} = v_F (k_x \sigma_x + \tau_z k_y \sigma_y) + \lambda_{so} \tau_z \sigma_z s_z, \quad (43)$$

where the analytical expressions for Fermi velocity v_F and magnitude of intrinsic effective SOC λ_{so} are given in Eqs. (33) (42), whose explicit values are presented in Table I via FP calculations. In this sense, the low-energy effective Hamiltonian is completely identified. The above spinful low-energy effective Hamiltonian is invariant under the space inversion symmetry operation and time reversal symmetry operation with $T = i s_y \tau_x \hat{K}$.

III. LOW-ENERGY EFFECTIVE HAMILTONIAN FOR HONEYCOMB X-HALIDE (X=N-BI) MONOLAYERS

A. Low-energy Hilbert subspace and effective Hamiltonian without SOC

For the X-halide (X=N-Bi) systems, the outer shell orbitals of X labeled as Xs , Xp_x , Xp_y , Xp_z , and the outer shell orbitals of halogen labeled as HS , Hp_x , Hp_y , Hp_z with (H=F-I) are taken into account in the following derivation. As is shown in Fig. 1(a), there are two distinct sites A and B in the honeycomb lattice unit cell of X-halide (X=N-Bi) with full halogenation from both sides of the 2D X honeycomb sheet. Therefore, in the representation $[Xp_y^A, Xp_x^A, Xp_z^A, Hp_z^A, Hp_y^A, Hp_x^A, Hs^A, Xs^A, Xp_y^B, Xp_x^B, Xp_z^B, Hp_z^B, Hp_y^B, Hp_x^B, Hs^B, Xs^B]$ and at the K point, the total Hamiltonian with the nearest neighbor hopping considered in the Slater-Koster formalism (Appendix A) reads

$$H_0^{ha} = \begin{pmatrix} h_{0,11} & h_{0,12} \\ h_{0,12}^\dagger & h_{0,11} \end{pmatrix}, \quad (44)$$

Eq. (5), as well as the following unitary transformation

$$h_{0,11} = \begin{pmatrix} 0 & 0 & 0 & 0 & V_{pp\pi}^{ha} & 0 & 0 & 0 \\ 0 & 0 & 0 & 0 & 0 & V_{pp\pi}^{ha} & 0 & 0 \\ 0 & 0 & 0 & V_{pp\sigma}^{ha} & 0 & 0 & -V_{sp\sigma}^{ha} & 0 \\ 0 & 0 & V_{pp\sigma}^{ha} & \Delta_p^{ha} & 0 & 0 & 0 & V_{sp\sigma}^{ha} \\ V_{pp\pi}^{ha} & 0 & 0 & 0 & \Delta_p^{ha} & 0 & 0 & 0 \\ 0 & V_{pp\pi}^{ha} & 0 & 0 & 0 & \Delta_p^{ha} & 0 & 0 \\ 0 & 0 & -V_{sp\sigma}^{ha} & 0 & 0 & 0 & \Delta_s^{ha} & V_{ss\sigma}^{ha} \\ 0 & 0 & 0 & V_{sp\sigma}^{ha} & 0 & 0 & V_{ss\sigma}^{ha} & \Delta \end{pmatrix}, \quad (45)$$

$$h_{0,12} = \begin{pmatrix} -V_1' & -iV_1' & 0 & 0 & 0 & 0 & 0 & V_2' \\ -iV_1' & V_1' & 0 & 0 & 0 & 0 & 0 & -iV_2' \\ 0 & 0 & 0 & 0 & 0 & 0 & 0 & 0 \\ 0 & 0 & 0 & 0 & 0 & 0 & 0 & 0 \\ 0 & 0 & 0 & 0 & 0 & 0 & 0 & 0 \\ 0 & 0 & 0 & 0 & 0 & 0 & 0 & 0 \\ 0 & 0 & 0 & 0 & 0 & 0 & 0 & 0 \\ -V_2' & iV_2' & 0 & 0 & 0 & 0 & 0 & 0 \end{pmatrix}, \quad (46)$$

$$h_{0,22} = \begin{pmatrix} 0 & 0 & 0 & 0 & V_{pp\pi}^{ha} & 0 & 0 & 0 \\ 0 & 0 & 0 & 0 & 0 & V_{pp\pi}^{ha} & 0 & 0 \\ 0 & 0 & 0 & V_{pp\sigma}^{ha} & 0 & 0 & V_{sp\sigma}^{ha} & 0 \\ 0 & 0 & V_{pp\sigma}^{ha} & \Delta_p^{ha} & 0 & 0 & 0 & -V_{sp\sigma}^{ha} \\ V_{pp\pi}^{ha} & 0 & 0 & 0 & \Delta_p^{ha} & 0 & 0 & 0 \\ 0 & V_{pp\pi}^{ha} & 0 & 0 & 0 & \Delta_p^{ha} & 0 & 0 \\ 0 & 0 & V_{sp\sigma}^{ha} & 0 & 0 & 0 & \Delta_s^{ha} & V_{ss\sigma}^{ha} \\ 0 & 0 & 0 & -V_{sp\sigma}^{ha} & 0 & 0 & V_{ss\sigma}^{ha} & \Delta \end{pmatrix}, \quad (47)$$

where Δ_p^{ha} is the on site energy for p_x , p_y , and p_z orbitals of halogen atoms, Δ (Δ_s^{ha}) is the on site energy for s orbital of X (halogen) atoms, the on site energies for p_x , p_y , and p_z orbitals of X atoms are taken to be zero. $V_{pp\pi}^{ha}$ ($V_{pp\sigma}^{ha}$) is the hopping between the p_z orbital from X and the p_z orbital from halogen atoms in the "shoulder by shoulder" ("head to tail") type. $V_{sp\sigma}^{ha}$ is the hopping between the p_z (s) orbital from X and the s (p_z) orbital from halogen atoms. $V_{ss\sigma}^{ha}$ is the hopping between the s orbital from X and the s orbital from halogen atoms. V_1' and V_2' can be expressed by the Slater-Koster parameters (Eq. (A5)).

Firstly, we perform the above unitary transformation

$$\begin{aligned} H\varphi_1^A &= -\frac{1}{\sqrt{2}} (Hp_x^A + iHp_y^A) \\ H\varphi_2^B &= \frac{1}{\sqrt{2}} (Hp_x^B - iHp_y^B) \\ H\varphi_3^A &= -\frac{1}{\sqrt{2}} (Hp_x^A - iHp_y^A) \\ H\varphi_4^B &= -\frac{1}{\sqrt{2}} (Hp_x^B + iHp_y^B) \end{aligned} \quad (48)$$

And then in new basis $[X\varphi_1^A, Xs^B, H\varphi_1^A, Hs^B, Xp_z^B, Hp_z^B, X\varphi_2^B, Xs^A, H\varphi_2^B, Hs^A, Xp_z^A, Hp_z^A, X\varphi_3^A, X\varphi_4^B, H\varphi_3^A, H\varphi_4^B] = [Xp_y^A, Xp_x^A, Xp_z^A, Hp_z^A, Hp_y^A, Hp_x^A, Hs^A, Xs^A, Xp_y^B, Xp_x^B, Xp_z^B, Hp_z^B, Hp_y^B, Hp_x^B, Hs^B, Xs^B] U_1^{ha}$, we rewrite the total Hamiltonian in the following block-diagonal form with three decoupled diagonal blocks

$$H_1^{ha} = H_{1,\alpha}^{ha} \oplus H_{1,\beta}^{ha} \oplus H_{1,\gamma}^{ha}, \quad (49)$$

$$H_{1,\alpha}^{ha} = \begin{pmatrix} 0 & iV_2 & V_{pp\pi}^{ha} & 0 & 0 & 0 \\ -iV_2 & \Delta & 0 & V_{ss\sigma}^{ha} & 0 & -V_{sp\sigma}^{ha} \\ V_{pp\pi}^{ha} & 0 & \Delta_p^{ha} & 0 & 0 & 0 \\ 0 & V_{ss\sigma}^{ha} & 0 & \Delta_s^{ha} & V_{sp\sigma}^{ha} & 0 \\ 0 & 0 & 0 & V_{sp\sigma}^{ha} & 0 & V_{pp\sigma}^{ha} \\ 0 & -V_{sp\sigma}^{ha} & 0 & 0 & V_{pp\sigma}^{ha} & \Delta_p^{ha} \end{pmatrix}, \quad (50)$$

$$H_{1,\beta}^{ha} = \begin{pmatrix} 0 & -iV_2 & V_{pp\pi}^{ha} & 0 & 0 & 0 \\ iV_2 & \Delta & 0 & V_{ss\sigma}^{ha} & 0 & V_{sp\sigma}^{ha} \\ V_{pp\pi}^{ha} & 0 & \Delta_p^{ha} & 0 & 0 & 0 \\ 0 & V_{ss\sigma}^{ha} & 0 & \Delta_s^{ha} & -V_{sp\sigma}^{ha} & 0 \\ 0 & 0 & 0 & -V_{sp\sigma}^{ha} & 0 & V_{pp\sigma}^{ha} \\ 0 & V_{sp\sigma}^{ha} & 0 & 0 & V_{pp\sigma}^{ha} & \Delta_p^{ha} \end{pmatrix}, \quad (51)$$

$$H_{1,\gamma}^{ha} = \begin{pmatrix} V_1 & 0 & \frac{V_{pp\pi}^{ha}}{\sqrt{2}} & \frac{V_{pp\pi}^{ha}}{\sqrt{2}} \\ 0 & -V_1 & -\frac{V_{pp\pi}^{ha}}{\sqrt{2}} & \frac{V_{pp\pi}^{ha}}{\sqrt{2}} \\ \frac{V_{pp\pi}^{ha}}{\sqrt{2}} & -\frac{V_{pp\pi}^{ha}}{\sqrt{2}} & \Delta_p^{ha} & 0 \\ \frac{V_{pp\pi}^{ha}}{\sqrt{2}} & \frac{V_{pp\pi}^{ha}}{\sqrt{2}} & 0 & \Delta_p^{ha} \end{pmatrix}. \quad (52)$$

For the first diagonal block $H_{1,\alpha}^{ha}$, in the presentation $\{X\varphi_1^A, Xs^B, H\varphi_1^A, Hs^B, Xp_z^B, Hp_z^B\}$ its eigenvectors can

be written as

$$|\varepsilon_i^{ha}\rangle = \frac{1}{N_i^{ha}} \times \begin{pmatrix} 1 \\ \frac{i}{V_{pp\pi}^{ha}} \\ \frac{\varepsilon_i^{ha} - \Delta_p^{ha}}{V_{pp\pi}^{ha}} \\ \frac{i[V_{pp\sigma}^{ha}(V_{sp\sigma}^{ha2} + V_{pp\sigma}^{ha}V_{ss\sigma}^{ha}) - \varepsilon_i^{ha}V_{ss\sigma}^{ha}(\varepsilon_i^{ha} - \Delta_p^{ha})]}{DC} \\ \frac{-iV_{sp\sigma}^{ha}[\Delta_s^{ha}V_{pp\sigma}^{ha} - \Delta_p^{ha}V_{ss\sigma}^{ha} - \varepsilon_i^{ha}(V_{pp\sigma}^{ha} - V_{ss\sigma}^{ha})]}{DC} \\ \frac{-iV_{sp\sigma}^{ha}[V_{sp\sigma}^{ha2} + V_{ss\sigma}^{ha}V_{pp\sigma}^{ha} - \varepsilon_i^{ha}(\varepsilon_i^{ha} - \Delta_s^{ha})]}{DC} \end{pmatrix}, \quad (53)$$

$$D(\varepsilon_i^{ha}) \equiv (\varepsilon_i^{ha} - \Delta_s^{ha}) [V_{pp\sigma}^{ha2} - \varepsilon_i^{ha}(\varepsilon_i^{ha} - \Delta_p^{ha})] + (\varepsilon_i^{ha} - \Delta_p^{ha}) V_{sp\sigma}^{ha2}, \quad (54)$$

$$C \equiv \frac{V_2(\varepsilon_i^{ha} - \Delta_p^{ha})}{V_{pp\pi}^{ha2} - \varepsilon_i^{ha}(\varepsilon_i^{ha} - \Delta_p^{ha})}, \quad (55)$$

where ε_i^{ha} and N_i^{ha} ($i = 1 - 6$) are the corresponding eigenvalues and the normalization factors, respectively. Therefore, upon performing the unitary transformation

$$\{\phi_1^{ha}, \phi_2^{ha}, \phi_3^{ha}, \phi_4^{ha}, \phi_5^{ha}, \phi_6^{ha}\} = \{X\varphi_1^A, Xs^B, H\varphi_1^A, Hs^B, Xp_z^B, Hp_z^B\} U_\alpha, \quad (56)$$

with $U_\alpha = \{|\varepsilon_i^{ha}\rangle\}_{i=1-6} \equiv \{u_{ji}^\alpha\}$, the above upper-left 6×6 diagonal block has been formally diagonalized.

From our FP calculations (Fig. 2(b)), the main components of the band around the Dirac points and the Fermi level come from the Xp_x and Xp_y orbitals, mixed with a small amount of the Hp_x and Hp_y orbitals and Xs orbital as well as other orbitals. The orbital features are identical with the eigenvectors of ε_1^{ha} , which is the linear combination of $\{X\varphi_1^A, Xs^B, H\varphi_1^A, Hs^B, Xp_z^B, Hp_z^B\}$, when we take its eigenvalue as the Fermi energy E_F . Similar to case of XH discussed in the previous section, from the perturbation theory, we can obtain the eigenvalues up to the second order correction and eigenvectors up to the first order correction

$$\varepsilon_1^{ha} = \frac{1}{2} \left(\Delta' + \sqrt{\Delta'^2 + 4V_2^2 - 2\frac{\Delta' V_{pp\pi}^{ha2}}{\varepsilon - \Delta_p^{ha}} + \frac{V_{pp\pi}^{ha4}}{(\varepsilon - \Delta_p^{ha})^2}} \right), \quad (57)$$

$$\begin{aligned} \Delta' &= \Delta - \\ &\frac{\varepsilon_1^{ha02}(V_{ss\sigma}^{ha2} + V_{sp\sigma}^{ha2}) - \varepsilon_1^{ha0}(\Delta_p^{ha}V_{ss\sigma}^{ha2} + \Delta_s^{ha}V_{sp\sigma}^{ha2})}{D(\varepsilon_i^{ha0})} + \\ &+ \frac{(V_{sp\sigma}^{ha2} + V_{ss\sigma}^{ha}V_{pp\sigma}^{ha})}{D(\varepsilon_i^{ha0})} \end{aligned} \quad (58)$$

$$\varepsilon_1^{ha0} = \frac{1}{2} \left(\Delta + \sqrt{\Delta^2 + 4V_2^2 - 2\frac{\Delta V_{pp\pi}^{ha2}}{\varepsilon - \Delta_p^{ha}} + \frac{V_{pp\pi}^{ha4}}{(\varepsilon - \Delta_p^{ha})^2}} \right), \quad (59)$$

$$\varepsilon = \frac{1}{2} \left(\Delta + \sqrt{\Delta^2 + 4V_2^2} \right). \quad (60)$$

Up to this point, we have found the low energy eigenvalue ε_1^{ha} (Eqs. (57) (58) (59) (60)) and the corresponding basis ϕ_1^{ha} (Eqs. (53) (54) (55) (56)).

However, from the above expressions, we checked that the rather lengthy correction terms in fact do not introduce interesting new physics. The main physics is already captured by the zeroth order eigenvalues and eigenvectors. So in the following, we take $\varepsilon_1^{ha} = \varepsilon_1^{ha0}$ and omit the first order correction $\{Hs^B, Xp_z^B, Hp_z^B\}$ for the eigenvector $\{|\varepsilon_1^{ha}\rangle\}$. Consequently, the eigenvector $\{|\varepsilon_1^{ha}\rangle\}$ reads with the following simple form in the basis $\{X\varphi_1^A, Xs^B, H\varphi_1^A\}$

$$|\varepsilon_1^{ha}\rangle = \frac{1}{n_1^{ha}} \begin{pmatrix} 1 \\ -i\frac{V_2}{\varepsilon_1^{ha0} - \Delta} \\ \frac{V_{pp\pi}^{ha}}{\varepsilon_1^{ha0} - \Delta_p^{ha}} \end{pmatrix} \equiv \begin{pmatrix} u_{11}^{ha} \\ u_{21}^{ha} \\ u_{31}^{ha} \end{pmatrix}, \quad (61)$$

with n_1^{ha} a normalized constant, and the eigenvalue ε_1^{ha0} given in Eqs. (59) and (60).

The eigenvalues of the second diagonal block $H_{1,\beta}^{ha}$ are denoted as ε_{6+i}^{ha} ($i = 1 - 6$), and satisfy $\varepsilon_{6+i}^{ha} = \varepsilon_i^{ha}$ ($i = 1 - 6$), where ε_i^{ha} ($i = 1 - 6$) are eigenvalues of $H_{1,\alpha}^{ha}$, since the two diagonal blocks have the same eigenequations. Through the similar processes, the low energy eigenvector $\{|\varepsilon_7^{ha}\rangle\}$ has the following simple form for the second diagonal block $H_{1,\beta}^{ha}$ in the basis $\{X\varphi_2^B, Xs^A, H\varphi_2^B\}$

$$|\varepsilon_7^{ha}\rangle = \frac{1}{n_1^{ha}} \begin{pmatrix} 1 \\ i\frac{V_2}{\varepsilon_1^{ha0} - \Delta} \\ \frac{V_{pp\pi}^{ha}}{\varepsilon_1^{ha0} - \Delta_p^{ha}} \end{pmatrix} = \begin{pmatrix} u_{11}^{ha} \\ -u_{21}^{ha} \\ u_{31}^{ha} \end{pmatrix}. \quad (62)$$

The third diagonal block $H_{1,\gamma}^{ha}$ contributes to the high energy Hilbert subspace, which does not interest us. Therefore, we do not need to diagonalize this diagonal block, although its diagonalization can be performed readily.

From the above analysis, the low-energy states ϕ_1^{ha} and ϕ_7^{ha} , which constitute the low-energy Hilbert subspace, have explicit forms after the above procedures of simpli-

fication

$$\begin{aligned}
\phi_1^{ha} &= u_{11}^{ha} \left[-\frac{1}{\sqrt{2}} (Xp_x^A + iXp_y^A) \right] + u_{21}^{ha} Xs^B \\
&\quad + u_{31}^{ha} \left[-\frac{1}{\sqrt{2}} (Hp_x^A + iHp_y^A) \right], \\
\phi_7^{ha} &= u_{11}^{ha} \left[\frac{1}{\sqrt{2}} (Xp_x^B - iXp_y^B) \right] - u_{21}^{ha} Xs^A \\
&\quad + u_{31}^{ha} \left[\frac{1}{\sqrt{2}} (Hp_x^B - iHp_y^B) \right].
\end{aligned} \tag{63}$$

We are interested in the low-energy physics near the Dirac point K , hence we perform the small \vec{k} expansion in the above low-energy Hilbert subspace around K by $\vec{k} \rightarrow \vec{k} + K$ and keep the first order term of \vec{k} ,

$$H_K = \begin{pmatrix} 0 & v_F k_- \\ v_F k_+ & 0 \end{pmatrix}, \tag{64}$$

with v_F the Fermi velocity

$$v_F = \frac{\sqrt{3}a}{2} \left[\frac{1}{2} |u_{11}^{ha}|^2 (V_{pp\sigma} - V_{pp\pi}) + |u_{21}^{ha}|^2 V_{ss\sigma} \right]. \tag{65}$$

Notice that for the X-halide (X=N-Bi) systems, $|u_{11}^{ha}|^2$ is much larger than $|u_{21}^{ha}|^2$ and $|u_{31}^{ha}|^2$. Through the analogical operations, around the Dirac point K' , we can obtain the low-energy Hilbert subspace

$$\begin{aligned}
\phi_1^{ha} &= u_{11}^{ha} \left[-\frac{1}{\sqrt{2}} (Xp_x^A - iXp_y^A) \right] - u_{21}^{ha} Xs^B \\
&\quad + u_{31}^{ha} \left[-\frac{1}{\sqrt{2}} (Hp_x^A - iHp_y^A) \right], \\
\phi_7^{ha} &= u_{11}^{ha} \left[\frac{1}{\sqrt{2}} (Xp_x^B + iXp_y^B) \right] + u_{21}^{ha} Xs^A \\
&\quad + u_{31}^{ha} \left[\frac{1}{\sqrt{2}} (Hp_x^B + iHp_y^B) \right],
\end{aligned} \tag{66}$$

and low-energy effective Hamiltonian

$$H_{K'} = \begin{pmatrix} 0 & v_F k_+ \\ v_F k_- & 0 \end{pmatrix}. \tag{67}$$

The low-energy effective Hamiltonian around the Dirac points K and K' are related by time reversal and space inversion symmetries. Finally, the low-energy Hilbert subspace can be chosen as

$$\begin{aligned}
\phi_1^{ha} &= u_{11}^{ha} \left[-\frac{1}{\sqrt{2}} (Xp_x^A + i\tau_z Xp_y^A) \right] + u_{21}^{ha} \tau_z Xs^B \\
&\quad + u_{31}^{ha} \left[-\frac{1}{\sqrt{2}} (Hp_x^A + i\tau_z Hp_y^A) \right], \\
\phi_7^{ha} &= u_{11}^{ha} \left[\frac{1}{\sqrt{2}} (Xp_x^B - i\tau_z Xp_y^B) \right] - u_{21}^{ha} \tau_z Xs^A \\
&\quad + u_{31}^{ha} \left[\frac{1}{\sqrt{2}} (Hp_x^B - i\tau_z Hp_y^B) \right].
\end{aligned} \tag{68}$$

and the low-energy effective Hamiltonian without SOC reads

$$H_\tau = v_F (k_x \sigma_x + \tau_z k_y \sigma_y), \tag{69}$$

where Pauli matrix σ denotes orbital basis degrees of freedom ϕ_1^{ha} and ϕ_7^{ha} , and τ_z labels valley index K and K' . Note that under the space reversal operation $P = \sigma_x \tau_x$ and the time reversal operation $T = \tau_x \hat{K}$, the above low-energy effective Hamiltonian (Eq. (69)) is also invariant.

B. Low-energy effective Hamiltonian involving SOC

In a similar way as in the previous section, a straightforward derivation leads to the on-site SOC in the spinful low-energy Hilbert subspace (Eq. (68)) $\{\phi_1, \phi_7\} \otimes \{\uparrow, \downarrow\}$,

$$H_{so} = \lambda_{so} \tau_z \sigma_z s_z, \tag{70}$$

$$\lambda_{so} = \frac{1}{2} |u_{11}^{ha}|^2 \xi_0^X + \frac{1}{2} |u_{31}^{ha}|^2 \xi_0^{ha}, \tag{71}$$

where u_{11}^{ha} and u_{31}^{ha} are given in Eq. (61), and ξ_0^X (ξ_0^{ha}) is magnitude of atomic SOC of pnictogen (halogen). It should be noted that the first order on site effective SOC also dominates in the X-halide (X=N-Bi) systems.

From the above Hamiltonian Eqs. (69) and (70) we obtain the generic low-energy effective Hamiltonian around the Dirac points acting on the low-energy Hilbert subspace (Eq. (68)) $\{\phi_1, \phi_7\} \otimes \{\uparrow, \downarrow\}$

$$H_{eff} = H_\tau + H_{so} = v_F (k_x \sigma_x + \tau_z k_y \sigma_y) + \lambda_{so} \tau_z \sigma_z s_z, \tag{72}$$

where Fermi velocity v_F and magnitude of intrinsic effective SOC λ_{so} are given in Eqs. (65) and (71), whose values are presented in Table II. The above spinful low-energy effective Hamiltonian is also invariant under the space inversion symmetry and time reversal symmetry with $T = i s_y \tau_x \hat{K}$.

IV. A SIMPLE SPINFUL LATTICE HAMILTONIAN FOR THE HONEYCOMB X-HYDRIDE/HALIDE (X=N-BI) MONOLAYERS

For the purpose of studying the topological properties of the honeycomb X-hydride/halide (X=N-Bi) monolayers, as well as their edge states, it is convenient to work with a lattice Hamiltonian via lattice regularization of the low-energy continuum models (Eq. (43) and Eq. (72)). Taking into account the main physics involving p_x and p_y orbitals, we derive the following spinful lattice Hamiltonian for the 2D honeycomb X-hydride/halide (X=N-Bi) monolayers

$$\begin{aligned}
H &= \sum_{\langle i,j \rangle; \alpha, \beta = p_x, p_y} t_{ij}^{\alpha\beta} c_{i\alpha}^\dagger c_{j\beta} \\
&\quad + \sum_{i; \alpha, \beta = p_x, p_y; \sigma, \sigma' = \uparrow, \downarrow} \lambda_{\sigma, \sigma'}^{\alpha\beta} c_{i\alpha\sigma}^\dagger c_{i\beta\sigma'} s_{\sigma, \sigma'}^z,
\end{aligned} \tag{73}$$

TABLE II. The parameters Fermi velocity v_F and magnitude of intrinsic effective SOC λ_{so} for honeycomb X-halide (X=N-Bi) monolayers, which are obtained from FP calculations. Note that $\lambda_{so} = E_g/2$, with E_g gap opened by SOC at the Dirac point.

system	v_F ($10^5 m/s$)	λ_{so} (eV)	system	v_F ($10^5 m/s$)	λ_{so} (eV)
NF	5.5	8.5×10^{-3}	NBr	4.2	19×10^{-3}
PF	7.2	13×10^{-3}	PBr	8.0	17×10^{-3}
AsF	7.3	80×10^{-3}	AsBr	8.2	98×10^{-3}
SbF	6.6	0.16	SbBr	7.7	0.20
BiF	7.2	0.55	BiBr	7.3	0.65
NCl	4.3	9.7×10^{-3}	NI	3.8	28×10^{-3}
PCl	7.8	17×10^{-3}	PI	8.1	19×10^{-3}
AsCl	8.0	95×10^{-3}	AsI	9.1	0.10×10^{-3}
SbCl	7.3	0.19	SbI	7.7	0.21
BiCl	6.9	0.56	BiI	7.7	0.65

where $\langle \rangle$ means nearest neighbor, α, β label orbital index, and Pauli matrix s^z stands for spin. The first term is the nearest neighbor hopping, and the second one is the on site SOC term, which is different from the SOC term in Kane-Mele model. Only the four spinful bands in the vicinity of Fermi level can capture low-energy long-wavelength properties of these systems.

After the Fourier transformation on the above simple lattice Hamiltonian, the model Hamiltonian and its energy spectrum over the entire Brillouin zone can be obtained. Since here spin is good quantum number, we can divide the model Hamiltonian into two sectors for spin up and down respectively. For spin up $s_z = 1$ and spin down $s_z = -1$ in the basis $\{p_x^A, p_y^A, p_x^B, p_y^B\}$, the corresponding model Hamiltonian reads

$$H^\uparrow(k) = \begin{pmatrix} 0 & -\frac{i\xi_0}{2} & h_{xx}^{AB}(k) & h_{xy}^{AB}(k) \\ 0 & h_{xy}^{AB}(k) & h_{xy}^{AB}(k) & h_{yy}^{AB}(k) \\ \dagger & 0 & -\frac{i\xi_0}{2} & 0 \end{pmatrix}, \quad (74)$$

$$H^\downarrow(k) = \begin{pmatrix} 0 & \frac{i\xi_0}{2} & h_{xx}^{AB}(k) & h_{xy}^{AB}(k) \\ 0 & h_{xy}^{AB}(k) & h_{xy}^{AB}(k) & h_{yy}^{AB}(k) \\ \dagger & 0 & \frac{i\xi_0}{2} & 0 \end{pmatrix}, \quad (75)$$

$$h_{xx}^{AB}(k) \equiv \frac{1}{2} (3V_{pp\sigma} + V_{pp\pi}) \cos\left(\frac{k_x}{2}\right) \exp\left(i\frac{k_y}{2\sqrt{3}}\right) + V_{pp\pi} \exp\left(-i\frac{k_y}{\sqrt{3}}\right),$$

$$h_{xy}^{AB}(k) \equiv i\frac{\sqrt{3}}{2} (V_{pp\sigma} - V_{pp\pi}) \sin\left(\frac{k_x}{2}\right) \exp\left(i\frac{k_y}{2\sqrt{3}}\right),$$

$$h_{yy}^{AB}(k) \equiv \frac{1}{2} (V_{pp\sigma} + 3V_{pp\pi}) \cos\left(\frac{k_x}{2}\right) \exp\left(i\frac{k_y}{2\sqrt{3}}\right) + V_{pp\sigma} \exp\left(-i\frac{k_y}{\sqrt{3}}\right).$$

For simplicity, we choose the lattice constant $a = 1$. The on site energies for p_x , p_y , and p_z orbitals are taken to be zero. ξ_0 is magnitude of atomic SOC of pnictogen. It should be noted that near the K and K' , the above model Hamiltonian (Eq. (74) and Eq. (75)) reduces to the low-energy effective Hamiltonian (Eq. (43) and Eq. (72)) with $v_F = \frac{\sqrt{3}a}{4} (V_{pp\sigma} - V_{pp\pi})$ and $\lambda_{so} = \frac{1}{2}\xi_0$.

V. DISCUSSION AND SUMMARY

For the X-hydride and X-halide (X=N-Bi) systems, we have obtained the low-energy effective Hamiltonian, which is analogous to the first proposal of the QSH effect¹² by Kane and Mele for graphene. The important difference is that in Kane-Mele model the effective SOC is of second order NNN type which is much weaker than the current on site SOC. The SOC mass term in the Hamiltonian opens a nontrivial gap at the Dirac points. Moreover, from K to K' the mass term changes its sign for spin up and spin down respectively, and the band is inverted. Therefore, QSH effect can be realized in the X-hydride and X-halide (X=N-Bi) monolayers. Some of these materials, such as BiH/BiF, have huge SOC gap with magnitude around 1eV when the Fermi energy is located inside the gap and the temperature is below the minimal gap energy. The energy spectrum of the total low-energy effective Hamiltonian is $E(\vec{k}) = \pm \sqrt{v_F^2 k^2 + \lambda_{so}^2}$ with a gap $E_g = 2\lambda_{so}$ at the Dirac points.

It is known that p_z orbital from carbon atom makes up the low-energy Hilbert subspace for Kane and Mele's first graphene QSH effect lattice Hamiltonian, where the NNN second order effective SOC term is introduced with the vanishing intraatomic on site SOC as well as the symmetry-forbidden nearest neighbor SOC. However, for the honeycomb X-hydride/halide (X=N-Bi) monolayers, p_x, p_y orbitals from the group V elements constitute the low-energy Hilbert subspace. This is the first class of materials for which the Dirac fermion physics is associated with p_x and p_y orbitals. It is because of this that the

effective on site SOC can have nonzero matrix elements and results in the huge SOC gap at the Dirac points. The effective on site SOC dominates in these systems. Analogous to the silicene, the NNN intrinsic Rashba SOC also exists here due to the broken mirror symmetry with respect to the x-y plane²⁵.

The leading order effective SOC processes in the X-hydride and X-halide (X=N-Bi) systems, low-buckled silicene, and graphene are schematically shown in Fig. 3. As shown in Fig. 3(a),(b), the representative leading order effective SOC processes around the K point in the honeycomb X-hydride and X-halide (X=N-Bi) monolayers are

$$\begin{aligned} |p_{+\uparrow}^A\rangle &\xrightarrow{\lambda_{so}} |p_{+\uparrow}^A\rangle, |p_{+\downarrow}^A\rangle \xrightarrow{-\lambda_{so}} |p_{+\downarrow}^A\rangle, \\ |p_{-\uparrow}^B\rangle &\xrightarrow{-\lambda_{so}} |p_{-\uparrow}^B\rangle, |p_{-\downarrow}^B\rangle \xrightarrow{\lambda_{so}} |p_{-\downarrow}^B\rangle, \end{aligned} \quad (76)$$

where λ_{so} represents the atomic spin-orbit interaction strength, which is given in Eq. (42) for X-hydride (X=N-Bi) systems and Eq. (71) for X-halide (X=N-Bi) systems. In the new low energy Hilbert subspace mainly consisted of p_x and p_y orbitals, the SOC arises in the first order on site processes, which leads to its huge magnitude. As a comparison, we also present the processes that lead to the leading order effective SOC in silicene and graphene, which are shown in Fig. 3(c),(d). The typical leading order (first order) NNN effective SOC process around the Dirac K point in silicene is given by²⁵

$$\begin{aligned} |p_{z\uparrow}^A\rangle &\xrightarrow{V} |p_{-\uparrow}^B\rangle \xrightarrow{-\frac{\xi_0}{2}} |p_{-\uparrow}^B\rangle \xrightarrow{V} |p_{z\uparrow}^A\rangle, \\ |p_{z\downarrow}^A\rangle &\xrightarrow{V} |p_{-\downarrow}^B\rangle \xrightarrow{\frac{\xi_0}{2}} |p_{-\downarrow}^B\rangle \xrightarrow{V} |p_{z\downarrow}^A\rangle, \\ |p_{z\uparrow}^B\rangle &\xrightarrow{V} |p_{+\uparrow}^A\rangle \xrightarrow{\frac{\xi_0}{2}} |p_{+\uparrow}^A\rangle \xrightarrow{V} |p_{z\uparrow}^B\rangle, \\ |p_{z\downarrow}^B\rangle &\xrightarrow{V} |p_{+\downarrow}^A\rangle \xrightarrow{-\frac{\xi_0}{2}} |p_{+\downarrow}^A\rangle \xrightarrow{V} |p_{z\downarrow}^B\rangle, \end{aligned} \quad (77)$$

where V represents the nearest neighbor direct hopping, ξ_0 represents the atomic intrinsic SOI strength. The whole process can be divided to three steps. As a representative example, we consider p_z^A orbital. Firstly, due to the low-buckled structure, p_z^A couples to p_-^B . Carriers in p_z^A orbital directly hops to the nearest neighbor p_-^B orbital. Secondly, when the atomic intrinsic SOC plays a role, the energy of p_-^B will split with spin up carriers shifting by $-\frac{\xi_0}{2}$ while spin down carriers shifting by $\frac{\xi_0}{2}$. In the third step, carriers in p_-^B directly hops to another nearest neighbor p_+^A orbital. For graphene, the typical leading order (second order) NNN effective SOC process around the Dirac K point is summarized as

$$\begin{aligned} |p_{z\uparrow}^A\rangle &\xrightarrow{\xi_0/\sqrt{2}} |p_{+\downarrow}^A\rangle \xrightarrow{V} |s_{\downarrow}^B\rangle \xrightarrow{V} |p_{+\downarrow}^A\rangle \xrightarrow{\xi_0/\sqrt{2}} |p_{z\uparrow}^A\rangle, \\ |p_{z\downarrow}^A\rangle &\xrightarrow{\xi_0/\sqrt{2}} |p_{-\uparrow}^A\rangle \xrightarrow{V} |s_{\uparrow}^B\rangle \xrightarrow{V} |p_{-\uparrow}^A\rangle \xrightarrow{\xi_0/\sqrt{2}} |p_{z\downarrow}^A\rangle. \end{aligned} \quad (78)$$

During the whole NNN hopping process, the atomic SOC appears twice. Thus, the effective SOC is of second order in ξ_0 .

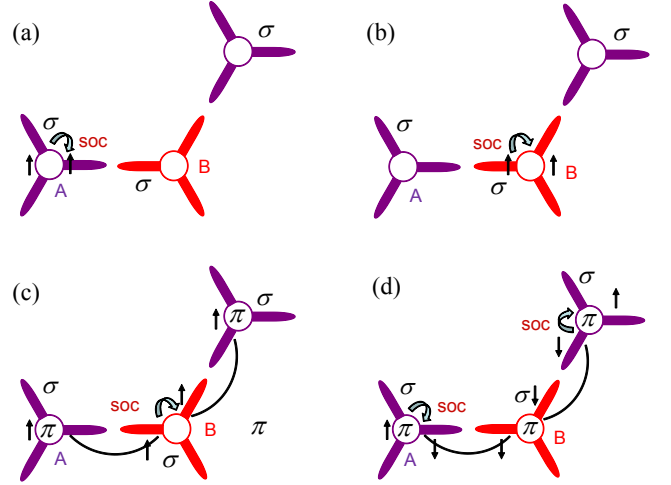


FIG. 3. (color online). The leading order effective SOC processes in X-hydride or X-halide (X=N-Bi), silicene and graphene. (a),(b) Sketches of the huge effective on site SOC in X-hydride (X=N-Bi) systems and X-halide (X=N-Bi) systems. (c) Sketch of the effective SOC from NNN hopping processes caused by the buckling in silicene. (d) Sketch of the second order effective SOC from NNN hopping processes in graphene.

In summary, through the tight binding method and our FP calculation, we derived the low-energy effective Hilbert subspace and Hamiltonian for the honeycomb X-hydride/halide (X=N-Bi) monolayers. These two types of 2D group V honeycomb lattice systems have the same low-energy effective Hamiltonian Eq. (43) and Eq. (72) due to their same D_{3d} point group symmetry and the same D_3 small group at the Dirac points. The two corresponding parameters v_F as well as λ_{so} , which have been obtained explicitly in Eqs. (33) (42) (65) (71) and are also obtained from FP calculations, are slightly different between the two types of systems due to their specific material details. Moreover, their low-energy Hilbert subspace is mainly consisted of p_x , p_y orbitals from the group V elements, which results in a huge on site SOC gap, which is distinct from the group IV honeycomb lattice monolayers such as silicene and graphene. Finally, a spinful lattice Hamiltonian with the on site SOC term for the 2D honeycomb X-hydride/halide (X=N-Bi) monolayers is proposed, which will be very useful for further investigations of this intriguing class of materials.

ACKNOWLEDGMENTS

This work was supported by the MOST Project of China (Nos. 2014CB920903, 2010CB833104, and 2011CBA00100), the National Natural Science Foundation of China (Grant Nos. 11225418, 51171001, and 11174337), SUTD-SRG-EPD2013062, and the Specialized Research Fund for the Doctoral Program of Higher

TABLE III. The matrix elements for the nearest neighbor hopping between s and p orbitals are considered as functions of the direction cosine l , m and n of the vector from the left orbital to the right orbital. Other matrix elements are found by permuting indices.

$t_{s,s}$	$V_{ss\sigma}$	$t_{x,x}$	$l^2 V_{pp\sigma} + (1-l^2) V_{pp\pi}$
$t_{s,x}$	$l V_{sp\sigma}$	$t_{x,y}$	$lm(V_{pp\sigma} - V_{pp\pi})$
$t_{x,s}$	$-l V_{sp\sigma}$	$t_{y,z}$	$mn(V_{pp\sigma} - V_{pp\pi})$

Education of China (Grant Nos. 20121101110046, and 20130001110002). Cheng-Cheng Liu was supported Excellent young scholars Research Fund of Beijing Institute of Technology (Grant No. 2013YR1816).

Appendix A: H_0 Matrix

Taking into account all the outer valence orbitals, the Hamiltonian with the nearest hopping in lattice space reads

$$H_0 = \sum_{i;\alpha} c_{i\alpha}^\dagger \epsilon_\alpha c_{i\alpha} + \sum_{\langle i,j \rangle; \alpha, \beta} c_{i\alpha}^\dagger t_{ij}^{\alpha\beta} c_{j\beta}, \quad (\text{A1})$$

$$t_{ij}^{\alpha\beta} \equiv \int d^3 \vec{r} \phi_\alpha^* (\vec{r} - \vec{R}_i) \hat{H}_0 \phi_\beta (\vec{r} - \vec{R}_j), \quad (\text{A2})$$

where α, β and i, j labels the orbital and site index, and the energy integral $t_{ij}^{\alpha\beta}$ can be considered in the Slater-Koster framework³², and ϵ_α is on site energy. The nearest hopping $t_{ij}^{\alpha\beta}$ is given in Table III by the Slater-Koster formula.

After the Fourier transformation the above Hamiltonian is written as

$$H_0 = \sum_{\alpha, \vec{k}} \epsilon_\alpha \left(a_i^\dagger (\vec{k}) a_i (\vec{k}) + b_i^\dagger (\vec{k}) b_i (\vec{k}) \right) + \sum_{\alpha\beta, \vec{k}} t^{\alpha\beta} (\vec{k}) a_\alpha^\dagger (\vec{k}) b_\beta (\vec{k}) + h.c., \quad (\text{A3})$$

$$t^{\alpha\beta} (\vec{k}) \equiv \sum_{\vec{d}^A} t^{\alpha\beta} (\vec{d}^A) e^{i\vec{k} \cdot \vec{d}^A}, \quad (\text{A4})$$

with \vec{d}^A being the nearest vectors. We choose the primitive vectors and nearest vectors as $\vec{a}_1 = a \left(\frac{1}{2}, \frac{\sqrt{3}}{2} \right)$, $\vec{a}_2 = a \left(-\frac{1}{2}, \frac{\sqrt{3}}{2} \right)$, $\vec{d}_1^A = \frac{a}{\sqrt{3}} \left(\frac{\sqrt{3}}{2}, \frac{1}{2} \right)$, $\vec{d}_2^A = \frac{a}{\sqrt{3}} \left(-\frac{\sqrt{3}}{2}, \frac{1}{2} \right)$, $\vec{d}_3^A = \frac{a}{\sqrt{3}} (0, -1)$. Therefore, every element in the above matrix (Eq. (A3)) at the Dirac points K and K' can be obtained in the Slater-Koster framework. The elements in Eq. (1) and Eq. (44) read

$$V_1' \equiv \frac{3}{4} (V_{pp\pi} - V_{pp\sigma}), V_2' \equiv \frac{3}{2} V_{sp\sigma}. \quad (\text{A5})$$

- ¹ A. K. Geim and K. S. Novoselov, Nature Mater. **6**, 183-191 (2007).
- ² A. H. Castro Neto, F. Guinea, N. M. R. Peres, K. S. Novoselov, and A. K. Geim, Rev. Mod. Phys. **81**, 109 (2009).
- ³ P. Vogt, P. De Padova, C. Quaresima, J. Avila, E. Frantzeskakis, M. C. Asensio, A. Resta, B. Ealet, and G. Le Lay, Phys. Rev. Lett. **108**, 155501 (2012).
- ⁴ L. Chen, C.-C. Liu, B. Feng, X. He, P. Cheng, Z. Ding, S. Meng, Y. Yao, and K. Wu, Phys. Rev. Lett. **109**, 056804 (2012).
- ⁵ Z. Song, C.-C. Liu, J. Yang, J. Han, B. Fu, Y. Yang, Q. Niu, J. Lu, and Y.G. Yao, arXiv:cond-mat/1402.2399.
- ⁶ C. Wu, D. Bergman, L. Balents, and S. Das Sarma, Phys. Rev. Lett. **99**, 070401 (2007).
- ⁷ C. Wu, Phys. Rev. Lett. **100**, 200406 (2008).
- ⁸ C. Wu, Phys. Rev. Lett. **100**, 200406 (2008).
- ⁹ M. Z. Hasan and C. L. Kane, Rev. Mod. Phys. **82**, 3045 (2010).
- ¹⁰ X. Qi and S. Zhang, Rev. Mod. Phys. **83**, 1057 (2011).
- ¹¹ B. Yan and S.-C. Zhang, Rep. Prog. Phys. **75**, 096501 (2012).
- ¹² C. L. Kane and E. J. Mele, Phys. Rev. Lett. **95**, 226801 (2005).
- ¹³ C. L. Kane and E. J. Mele, Phys. Rev. Lett. **95**, 146802 (2005).
- ¹⁴ Y. G. Yao, F. Ye, X. L. Qi, S. C. Zhang, and Z. Fang, Phys. Rev. B **75**, 041401(R) (2007).
- ¹⁵ H. Min, J. E. Hill, N. A. Sinitsyn, B. R. Sahu, L. Kleinman, and A. H. MacDonald, Phys. Rev. B **74**, 165310 (2006).
- ¹⁶ B. A. Bernevig, T. L. Hughes, and S. C. Zhang, Science **314**, 1757-1761 (2006).
- ¹⁷ M. König, S. Wiedmann, C. Brüne, A. Roth, H. Buhmann, L. W. Molenkamp, X. L. Qi, and S.C. Zhang, Science **318**, 766-770 (2007).
- ¹⁸ C. X. Liu, T. L. Hughes, X. L. Qi, K. Wang, and S. C. Zhang, Phys. Rev. Lett. **100**, 236601 (2008).
- ¹⁹ I. Knez, R.R. Du, and G. Sullivan, Phys. Rev. Lett. **107**, 136603 (2011).
- ²⁰ I. Knez, R.R. Du, and G. Sullivan, Phys. Rev. Lett. **109**, 186603 (2012).
- ²¹ S. Murakami, Phys. Rev. Lett. **97**, 236805 (2006).
- ²² Z. Liu, C. X. Liu, Y.S. Wu, W.H. Duan, F. Liu, and Jian Wu, Phys. Rev. Lett. **107**, 136805 (2011).
- ²³ T. Hirahara, G. Bihlmayer, Y. Sakamoto, M. Yamada, H. Miyazaki, S.I. Kimura, S. Blügel, and S. Hasegawa, Phys. Rev. Lett. **107**, 166801 (2011).
- ²⁴ C.-C. Liu, W. Feng, and Y. Yao, Phys. Rev. Lett. **107**, 076802 (2011).
- ²⁵ C.-C. Liu, H. Jiang, and Y. Yao, Phys. Rev. B **84**, 195430 (2011).
- ²⁶ C. Weeks, J. Hu, J. Alicea, M. Franz, and R. Wu, Phys.

- Rev. X **1**, 021001 (2011).
- ²⁷ Y. Xu, B. Yan, H.-J. Zhang, J. Wang, G. Xu, P. Tang, W. Duan, and S.-C. Zhang, Phys. Rev. Lett. **111**, 136804 (2013).
- ²⁸ Z.F. Wang, Z. Liu, and F. Liu, Nat. Commun. **4**, 1471 (2013).
- ²⁹ F. Yang, L. Miao, Z. F. Wang, M.-Y. Yao, F. Zhu, Y. R. Song, M.-X. Wang, J.-P. Xu, A. V. Fedorov, Z. Sun, G. B. Zhang, C. Liu, F. Liu, D. Qian, C. L. Gao, and J.-F. Jia, Phys. Rev. Lett. **109**, 016801 (2012).
- ³⁰ M. Zhou, W. Ming, Z. Liu, Z. Wang, Y.G. Yao, and F. Liu, arXiv:cond-mat/1401.3392.
- ³¹ R. Shankar, *Principles of Quantum Mechanics* (Second Edition) (Plenum Press, New York and London, 1994).
- ³² J. C. Slater and G. F. Koster, Phys. Rev. **94**, 1498 (1954).